JACS
JOURNAL OF THE AMERICAN CHEMICAL SOCIETY

Article

pubs.acs.org/JACS

Crystallization, Melting, and Structure of Water Nanoparticles at Atmospherically Relevant Temperatures

Jessica C. Johnston and Valeria Molinero*

Department of Chemistry, University of Utah, Salt Lake City, Utah 84112-0850, United States

ABSTRACT: Water nanoparticles play an important role in atmospheric processes, yet their equilibrium and nonequilibrium liquid–ice phase transitions and the structures they form on freezing are not yet fully elucidated. Here we use molecular dynamics simulations with the mW water model to investigate the nonequilibrium freezing and equilibrium melting of water nanoparticles with radii R between 1 and 4.7 nm and the structure of the ice formed by crystallization at temperatures between 150 and 200 K. The ice crystallized in the particles is a hybrid form of ice I with stacked layers of the cubic and hexagonal ice polymorphs in a ratio approximately 2:1. The ratio of cubic ice to hexagonal ice is insensitive to the radius of the water particle and is comparable to that found in simulations of bulk water around the same temperature. Heating frozen particles that contain multiple crystallites leads to Ostwald ripening and annealing of the ice structures, accompanied by an increase in the amount of ice at the expense of the liquid water, before the particles finally melt from the hybrid ice I to liquid, without a transition to hexagonal ice. The melting temperatures T_m of the nanoparticles are not affected by the ratio of cubic to hexagonal layers in the crystal. T_m of the ice particles decreases from 255 to 170 K with the particle size and is well described by the Gibbs–Thomson equation, $T_m(R) = T_m^{bulk} - K_{GT}/(R-d)$, with constant $K_{GT} = 82 \pm 5$ K·nm and a premelted liquid of width $d = 0.26 \pm 0.05$ nm, about one monolayer. The freezing temperatures also decrease with the particles' radii. These results are important for understanding the composition, freezing, and melting properties of ice and liquid water particles under atmospheric conditions.

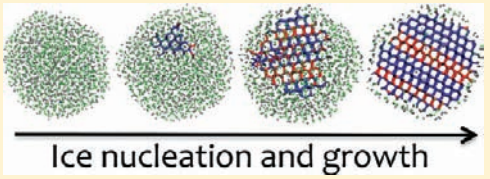

INTRODUCTION

Nanometer-sized particles of water play an important role in the atmosphere.[1−3] Atmospheric temperatures can be as low as 120 K in the polar mesosphere, from 180 to 200 K in the tropical tropopause, and up to 320 K.[4−8] It has been suggested that the mechanism of ice formation in the atmosphere follows Ostwald's step rule, in which crystallization occurs through the initial formation of metastable phases with smaller free energy barriers before reaching the lowest free energy phase.[9] For ice formation in clouds, the proposed mechanism for the formation of hexagonal ice follows this sequence of transitions: water vapor to liquid clusters to cubic ice clusters to hexagonal ice clusters.[10,11]

The structure of cubic ice, Ic, first assigned by Konig,[12] would be very similar to that of hexagonal ice, Ih, the stable bulk polymorph. Each water molecule in Ic and Ih is tetrahedrally coordinated to four neighbors through hydrogen bonds; the difference is that the four neighbors form staggered hydrogen bonds in cubic ice, while three neighbors form staggered bonds and one an eclipsed bond in hexagonal ice. Occurrence of the rare Schiener's halo, a 28° circular halo observed around the sun, has been attributed to the formation of cubic ice in the atmosphere.[8,13−15] Laboratory experiments of micrometer-sized water droplets at temperatures up to 243 K reveal the formation of crystals with the diffraction pattern of faulty cubic ice.[6,16] There is no evidence to date for the formation of pure cubic ice Ic.[16−25] Recent simulations and experimental studies of ice I obtained at very low temperatures indicate that, while the diffraction patterns of the ice formed from deeply supercooled water are almost the same as expected for the cubic ice polymorph, the crystals have a hybrid structure composed of a comparable fraction (about 1:2 to 2:1) of cubic and hexagonal ice layers arranged as short stacks of the two polymorphs.[6,17−19,21,26] The evidence toward a hybrid cubic/hexagonal structure for ice formed from deeply supercooled water raises the question to what extent does crystallization of small atmospheric water droplets result in ice Ic.

While there have been experimental studies investigating crystallization in water droplets, the size range of the droplets studied are mostly in the micrometer range, as it is difficult to prepare and characterize nanosized ice clusters without contact with a substrate.[3] Insight on the structure of water nanoclusters at cold temperatures has been obtained from expansion beam experiments.[3,27−35] The ice nanoparticles obtained in those beam expansion experiments did not show the diffraction pattern characteristic of hexagonal ice. Electron diffraction patterns of water clusters in the range of a couple hundred water molecules to several thousand water molecules have been interpreted to indicate the presence of cubic ice,[27−29] although several discrepancies with the expected diffraction pattern of ice Ic have been reported[29] and—we note—the diffraction patterns are also consistent with the signatures of the hybrid ice with stacks of cubic and hexagonal layers.

Crystallization of water particles in simulations has been limited to clusters with 20 molecules or less, which form specific ordered structures different from ice I;[36−40] larger water clusters vitrified under the cooling rates accessible to atomistic

Received: November 18, 2011
Published: March 27, 2012

   dx.doi.org/10.1021/ja210878c | J. Am. Chem. Soc. 2012, 134, 6650−6659

simulations. There is scarce experimental data on the nonequilibrium freezing temperatures and crystallization rates for water nanoparticles.[27,34,35] This is unsurprising in view of how challenging it is to characterize the size, temperature, and structure of the particles as they evolve in a molecular beam. The few experiments available indicate that the freezing temperatures for nanodroplets decrease with decreasing size of the particle and are considerably lower than the freezing temperatures for micrometer-sized droplets cooled at comparable rates.[27,34,35] The temperature dependence of the crystallization rate of water nanoparticles is not yet available.

The equilibrium melting temperatures of unsupported ice nanoparticles have not yet been determined in experiments. Melting of small water clusters, with 8−216 water molecules, has been studied through molecular simulations.[40] A recent molecular dynamics simulation study determined the melting temperature of nanoparticles of hexagonal ice with radius 1.5−4 nm using the TIP4P water model.[41] The simulations indicate that, for clusters with >20 molecules, the melting temperature decreases with decreasing size of the particles in a manner approximately inverse to their radius.[40,41] The actual structures of the ice nanoclusters formed under atmospherically relevant conditions have not yet been elucidated, nor has the influence of stacking faults on the melting of water nanoparticles.

In this work, we investigate the freezing and melting processes of water particles with radii in the range of about 1−5 nm using extensive molecular dynamics simulations. Our aim is to elucidate the structure of the ice formed in nanoparticles, to determine their nonequilibrium crystallization temperatures and equilibrium melting temperatures, and to shed light on the processes of nucleation and growth of ice and the ripening of the ice structures on heating. The study of freezing and melting of ice with molecular simulations requires the use of a model that is both accurate in representing the ice−liquid phase behavior of water and computationally efficient to tackle the long simulations required to characterize the melting and—most challenging—the homogeneous nucleation and growth of ice. In the present work, we use the coarse-grained monatomic water model mW, which represents each water molecule by a single particle with a three-body interaction that penalizes nontetrahedral angles.[42] The mW model encourages the formation of tetrahedral "hydrogen-bonded" configurations without the use of electrostatic interactions or explicit hydrogen atoms and is 180 times more computationally efficient than atomistic water models. Of relevance for the present work, mW correctly predicts the structure of liquid and crystalline states of water and the phase transformations between them.[19,24,42−45] The mW model predicts that bulk cubic ice Ic is metastable with respect to bulk hexagonal ice Ih (T_m^{Ih} = 274 K and T_m^{Ic} = 272 K in the mW model, in good agreement with the experimental (Ih) and predicted (Ic) values for these crystals[24,42]) and has been used to characterize the phase diagram of bulk and nanoconfined water[24,25,42,43,46,47] and to investigate the kinetics of crystallization of ice.[44,45] In what follows we use the mW water model to investigate the structure, freezing, and melting of water nanoparticles and discuss their state under atmospherically relevant temperatures.

METHODS

Molecular dynamics simulations were performed using LAMMPS[48] with the mW water model.[42] Equations of motion were integrated using the velocity Verlet algorithm with a time step of 10 fs. Constant temperature and cooling/heating simulations were evolved in the canonical (*NVT*) ensemble. Isoenergetic simulations were evolved in the microcanonical (*NVE*) ensemble. The temperature was controlled with a Nosé−Hoover thermostat with relaxation time 1 ps; the target temperature of the cooling (heating) ramps was decreased (increased) linearly with time. Each individual water particle was classified as being liquid or ice, based on the correlations of orientational order with respect to its four nearest neighbors using the CHILL algorithm;[24] molecules are classified according to whether they have the local order of cubic ice (C), hexagonal ice (H), interfacial or intermediate ice (I), or liquid water (L). For a detailed description of the algorithm and its parameters, we refer the reader to ref 24.

We prepared water clusters with N = 159, 417, 915, 2149, 4235, and 13824 water molecules which we equilibrated for 1 ns at 280 K, followed by an instantaneous quenching of the liquid clusters to 220 K. Twenty independent liquid configurations were generated for each of these clusters by evolving the N-sized liquid cluster at 220 K for 20 ns and selecting configurations every 1 ns. Although the next section shows that some of these liquid clusters are supercooled, we verified that crystallization does not occur during the 20 ns used to collect the configurations. The radii R were determined from the molecular volume of ice in the mW model, v = 30.6 Å^3, and the number N of water molecules in the particle, assuming that the particles were spherical, $R = (3vN/4\pi)^{1/3}$. The assumption of spherical particles is in good agreement with the results of the simulations. The radii ranged from 1.05 to 4.7 nm. Particles of pure hexagonal ice Ih and pure cubic ice Ic were created by cutting a sphere of radius R from the corresponding bulk ice lattices.

We examined the freezing of water nanoparticles through three types of simulation experiments: constant rate cooling simulations, isothermal simulations, and isoenergetic simulations. *Cooling ramps with constant rates* of 1, 0.5, 0.1, and 0.05 K ns^{-1} were used to determine the freezing temperature T_f^{max}, identified for each particle as the inflection point in the fraction of ice versus temperature at the fastest cooling rate that results in crystallization of the particle. The cooling rates were sufficiently slow that the particles were always in thermal equilibrium. At least 20 independent freezing simulations for particles of each radius were performed at various freezing rates, each starting at temperatures that were at least 20 K above the corresponding freezing points reported in next section. The simulation times for each of these cooling simulations spanned from 60 ns to 1 μs. Additional sets of *isothermal simulations* performed at T = 180 and 200 K—temperatures in the range important for tropopause and polar stratospheric clouds[6,8]—were used to characterize the structure of ice in the nanoparticles. We performed 20 independent isothermal simulations, each 100−400 ns long, at 180 K for each particle size with R ranging from 4.7 to 1.5 nm. We also performed 20 independent simulations, each 20−500 ns long, at 200 K for each of the particles with radius larger than 1.9 nm. Twenty additional isothermal simulations at 150 K, each 500 ns long, were performed for the ensemble of particles with R = 1.05 nm. *Isoenergetic* (microcanonical) simulations were performed on the particle with R = 4.7 nm at total energies selected through pre-equilibration of the liquid droplets at 170, 180, 185, 190, 195, 200, and 205 K for 0.1 ns. Each microcanonical simulation was evolved until the crystallization of the nanoparticles was complete, within 50 ns for the energies considered in this study.

Nucleation times were determined as the times elapsed before the onset of the appearance of growing ice nuclei, and growth times were determined as the time elapsed between the nucleation times and the completion of crystallization, evidenced by the onset of a plateau in the fraction of ice as a function of time. Melting temperatures T_m were determined by heating at 1 K ns^{-1} sets of 20 independent crystalline nanoparticles for each R size. The initial temperature was in all cases at least 25 K lower and the final temperature at least 20 K higher than the melting temperature of each particle reported in the next section, which was identified as the inflection point in the fraction of ice versus temperature on heating. Each melting simulation lasted between 60 and 100 ns. This work encompasses more than 360 independent simulations of freezing of water nanodroplets and 120 simulations of their melting.

dx.doi.org/10.1021/ja210878c | J. Am. Chem. Soc. 2012, 134, 6650−6659

RESULTS AND DISCUSSION

1. Freezing of Water Nanoparticles. The crystallization of liquid water requires the spontaneous creation and growth of ice nuclei. The time scale for nucleation decreases with increasing supercooling, while the time scale for the growth of the nuclei follows the opposite trend. This results in a temperature at which the crystallization rate of ice is maximum.[45] Molecular simulations and classical nucleation theory using experimental data for water indicate that the temperature of maximum crystallization rate, T_f^{max}, for bulk water occurs a few degrees below the experimental temperature of homogeneous nucleation and is controlled by the structural transformation of supercooled water into a mostly four-coordinated liquid.[45] In this section, we determine the temperature of maximum crystallization rates of water nanoparticles as a function of their radii, $T_f^{max}(R)$, and estimate the rates of ice crystallization.

We first determined the maximum cooling rate q^{max} that results in the crystallization of the liquid particles. To this effect, we performed a series of cooling temperature ramps with cooling rates q = 10, 1, 0.5, 0.1, and 0.05 K ns^{-1}. The q^{max} slowly decreases with the volume of the droplet, from 1 K ns^{-1} for R = 4.7 nm to 0.1 K ns^{-1} for R = 1.5 nm; the cluster with R = 1.05 nm did not crystallize even at 0.05 K ns^{-1} (Table 1). The freezing temperature at the fastest cooling rate that results in crystallization of each nanoparticle, the $T_f^{max}(R)$ shown in Table 1, corresponds to the temperature at which the rate of crystallization is maximum.[45] The temperatures of maximum crystallization rate of the water nanoparticles decrease with decreasing size, from T_f^{max} = 196 ± 2 K for R = 4.7 nm to 179 ± 3 K for R = 1.5 nm (Table 1 and Figure 1). These values are lower than for bulk mW water, $T_f^{bulk,max}$ = 202 K,[45] and evidence a continuous decrease of the temperature of maximum crystallization rate with confinement.

Table 1. Freezing and Melting Temperatures of Water Nanodroplets[a]

N waters	R (nm)	T_m (K)	T_m^{HEX} (K)	T_f^{max} (K)	q^{max} (K ns^{-1})
13824	4.7	255 ± 2	257 ± 3	196 ± 2	1
4235	3.1	245 ± 3	246 ± 3	192 ± 3	1
2149	2.5	237 ± 2	238 ± 3	190 ± 3	0.5
915	1.9	224 ± 2	224 ± 3	190 ± 2	0.1
417	1.5	205 ± 3	208 ± 3	179 ± 3	0.1
159	1.05	170 ± 9	162 ± 5	~155	<0.05

[a]The equilibrium melting temperature of particles with N water molecules and radius R with structure of hexagonal ice (T_m^{HEX}) and the hybrid ice I structure obtained by spontaneous crystallization of the particles (T_m) are indistinguishable within their error bars. Melting of the R = 4.7 nm pure cubic ice nanoparticles yields $T_m^{CUB}(R$ = 4.7 nm) = 256 ± 2, also indistinguishable from the hybrid and hexagonal ices. The temperatures of maximum crystallization rate (T_f^{max}) indicate the freezing temperature at the fastest cooling rate that produces ice, q^{max}. T_f^{max} for R = 1.05 nm is approximate because these particles did not crystallize at the slowest rate of this study.

$T_f^{max}(R)$ is an intrinsic, well-defined physical property for each nanoparticle size. Experimental freezing temperatures, however, are usually determined at an arbitrary rate q. The range of q^{max} changes only 1 order of magnitude as the radius decreases from 4.7 to 1.5 nm; therefore, we also determined the freezing temperature for R = 4.7 nm cooled at a rate q = 0.1 K ns^{-1} and found that is just 5 K higher than for q = 1 K ns^{-1}.

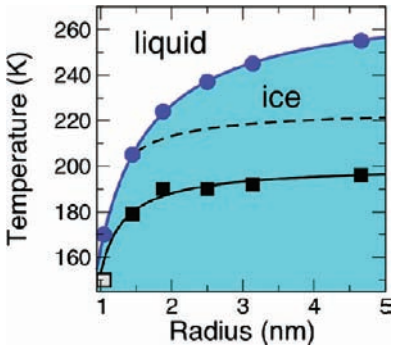

Figure 1. Temperature–radius phase diagram for the solid–liquid transformation in water nanoparticles. The equilibrium melting temperatures T_m (blue circles) and the nonequilibrium temperatures of maximum crystallization rate T_f^{max} (black squares) are well represented by Gibbs–Thomson equations (solid blue and black lines, respectively) with the parameters shown in the text. We were unable to determined a temperature of maximum freezing rate for R = 1.05 nm; the white square shows the T = 150 K at which these droplets were crystallized, within 500 ns, in the simulations. The dashed black line shows a line 25 K above the T_f^{max} determined with the mW model, which we conjecture may be a better estimation of the actual locus of T_f^{max} in real water based on the comparison and arguments presented for bulk water in ref 45.

This implies that the line of $T_f(R; q$ = 0.1 K ns$^{-1})$ is very close to the line of $T_f^{max}(R)$ reported in Figure 1, with a slightly more pronounced slope. While this work was under review, we learned of a then still unpublished experimental study by Wyslouzil and co-workers on the freezing of water nanodroplets, which—like the simulations of this study—indicated a decrease of freezing temperature with the radius of the nanoparticle: 215 K for $R \approx$ 5.8 nm, 214 K for $R \approx$ 4.3 nm, 205 K for $R \approx$ 3.5 nm, and 202 K for $R \approx$ 3.2 nm, measured at q = 4 × 10^{-4} K ns^{-1}.[35] The freezing temperatures measured in the supersonic nozzle are about 20 K above the corresponding $T_f^{max}(R)$ determined in the simulations. It is not feasible to cool the nanoparticles at 10^{-4} K ns^{-1} in the simulations, because of the associated computational cost. Based on the temperature dependence of the crystallization times of bulk mW water around T_f^{max},[45] we estimate that a reduction of the cooling rates from 1 to 10^{-4} K ns^{-1} would result in an increase of about 15 K in the freezing temperature of the mW water nanoparticles, in very good agreement with the experimental result. We note, however, that the experimental results are at a single rate q and the locus of $T_f^{max}(R)$ in experiments is not yet known.

We estimated the rate of crystallization of the nanoparticles from the volume V of the droplets and the times of crystallization τ_x, $J = 1/(\tau_x V)$. The crystallization rates for mW water nanoparticles at T_f^{max} are on the order of 10^{27} cm^{-3} s^{-1} and not very sensitive to particle size. Size independent J resulting from the scaling of the crystallization time τ_x with the inverse of the volume V of the droplet is not unexpected because the formation of ice is a stochastic process and—we show below—critical nuclei form across the volume of the clusters. Bartell and co-workers[27,34] measured crystallization for water clusters with about 800–6000 molecules near 200 K and determined rates of about 10^{24}–10^{25} cm^{-3} s^{-1}; Wyslouzil and co-workers investigated clusters of radii between 5.8 and 3.1 nm and found crystallization rates on the order of 10^{23} cm^{-3} s^{-1} for cooling rates 4 × 10^{-4} K ns^{-1}.[35] The lower value of J of the experiments compared to the simulations reflects the lower cooling rate in the former. The temperature dependence of the

dx.doi.org/10.1021/ja210878c | J. Am. Chem. Soc. 2012, 134, 6650–6659

ice crystallization rate, $J(T;R)$, is not yet available for water nanoparticles. We expect the maximum rates of ice crystallization $J^{max}(T_f^{max};R)$ for real water to be lower than predicted by the simulations,[44,45] because the maximum crystallization rate is proportional to the diffusion coefficient of the supercooled liquid,[45,49] which is overestimated by the mW water model.[42]

The water clusters with R = 1.05 nm did not crystallize even when cooled at the slowest rate of this study, 0.05 K ns^{-1}. Combined theoretical and experimental infrared spectroscopy studies of the OH stretching in water clusters rapidly cooled to 100 K indicated that clusters of less than about 1 nm radius contained no crystalline component,[31,50] and electron diffraction results suggested that the onset of crystallinity occurs at around 200 water molecules.[29] In qualitative agreement with these determinations, the critical water cluster radius for the transition from amorphous water to ice was estimated to be 1.0 ± 0.5 nm using classical nucleation theory with experimental bulk data.[10] Therefore, it was important to determine whether the small R = 1.05 nm clusters containing 159 molecules were able to produce ice in simulations. To this end, we instantaneously quenched to T = 150 K an ensemble of 20 R = 1.05 nm liquid particles and evolved them at that temperature for t = 500 ns, during which 85% of the droplets crystallized. The surface of each particle remained disordered, as previously found in atomistic simulations.[31,50] For the crystallized R = 1.05 nm droplets we find that only 19 ± 6% of the water (about 30 molecules) have the ordering of cubic or hexagonal ice, 27 ± 4% are in the form of the less ordered interfacial ice, and the other 55 ± 10% of the water molecules are in an amorphous/liquid state. The fraction of liquid is in excellent agreement with the width derived in section 3 for the premelted liquid layer around the crystallites, d = 0.26 ± 0.05 nm. To assess whether smaller water particles could form ice, we prepared an R = 1.0 nm cluster, with 137 molecules, and held it at 150 K. The cluster, originally hexagonal ice, melted immediately and within 55 ns nucleated a small hybrid crystallite containing ∼60 atoms (including interfacial ice) surrounded by a disordered premelted layer. The instability of hexagonal ice droplets containing ∼130 molecules was previously observed in atomistic simulations;[31,41,50] the more efficient coarse-grained simulations of this study, however, allow for longer sampling that reveals the subsequent crystallization of a tiny crystallite. A detailed look at the time evolution of the 1.0 nm radius cluster shows significant fluctuations in the size of the crystallite, which disappears and re-forms several times in time scales of several hundreds of nanoseconds. We note that the critical cluster size for the crystallization of bulk mW water around T_f^{max} contains ∼100 molecules (about half that number if the interfacial ice is not considered),[45,51,52] larger than the crystallites in the 1.05 and 1.0 nm particles at 150 K. Formation of a stable crystal is not possible when the confined volume is comparable to or smaller than the size of the critical nucleus.[53,54] Oscillations between crystal-like and liquid states as a function of time have been reported in simulations of atoms[55−59] and water[36−39] clusters containing less than 20 molecules. The oscillations arise from small free energy barriers separating these two states in small systems.[58] Different from the crystallites of the present study, ordered crystal-like isomers in these small water clusters are unrelated to ice I and have been reported to display unusually high ice−liquid equilibrium temperatures.[36−39] The large fluctuations in the fraction of ice in the 1.0 nm clusters suggest that the liquid−ice transition is already losing the first order character for those particles. We conclude that while droplets with as few as 137 molecules form a small crystalline core, smaller clusters with about 100 molecules are most probably unable to form ice I.

We find that the temperatures of maximum crystallization rate are well represented by the relation $T_f^{max}(R) = T_f^{bulk,max} - K_f/(R - d_f)$ with constant K_f = 20 K·nm and a correction to the radius of the particle d_f = 0.6 nm. This relation predicts $T_f^{max} \approx$ 155 K for the 1.05 nm droplets, very close to the temperature, 150 K, at which we observe crystallization of these smallest droplets within 500 ns. An identical functional form was found to describe the experimental depression in freezing point for water confined in cylindrical nanopores as a function of pore radius.[60,61] The relation between the freezing temperature and the particle radius has the same mathematical form as the modified Gibbs−Thomson equation, which describes the depression of the equilibrium melting temperature with particle size (see section 3) and is derived from *equilibrium* thermodynamics.[62,63] This may be puzzling because water freezing is a *nonequilibrium* process. It has been shown, however, that the freezing temperature of water is entirely determined by its chemical potential,[64] controlled by a sharp structural transformation of supercooled liquid water into a mostly four-coordinated liquid.[45]

2. Structure of the Crystallized Water Nanoparticles. We now turn our focus to the mechanisms of crystallization and structures of the ice obtained through freezing of the nanodroplets at constant temperature. A change in the mechanism of ice crystallization, from nucleation dominated at $T > T_f^{max}$ to growth dominated at $T < T_f^{max}$ was recently demonstrated in simulations of crystallization of bulk water.[45] For particles with R > 1.5 nm, the freezing temperature is between 180 and 200 K, resulting in different mechanisms of crystallization at these two temperatures. Crystallization at $T > T_f^{max}$ occurs after a transient nucleation period in which subcritical ice nuclei form and dissolve into the solution. For R = 2.5 nm, only 18 of 20 simulations crystallized after t = 500 ns at 200 K. As such, we did not perform simulations at 200 K for R < 2.5 nm because of the long time that would be necessary to observe nucleation. At 200 K, above T_f, the rate of crystallization of ice is controlled by the rate of nucleation, and once the critical nuclei form, the ice crystals grow rapidly. Crystallization at 200 K was always initiated by a single ice nucleus in each droplet, resulting in fewer and more ordered crystallites than those formed at 180 K. The nucleation and growth of ice in a R = 2.5 nm particle at 200 K is shown in the Abstract figure.

Below T_f^{max}, the rate of crystallization is controlled by the rate of growth of ice. For example, for R = 1.9 nm, for which T_f^{max} > 180 K, 70% of the water particles nucleated ice immediately at 180 K, and the average nucleation time (∼3 ns) was significantly shorter than the average growth time (∼17 ns), while for R = 1.5 nm, for which T_f^{max} < 180 K, the average nucleation time (∼40 ns) far exceeded the growth time (∼10 ns). Figure 2 illustrates the nucleation and growth of ice nuclei in a representative water particle with R = 4.7 nm at 180 K, below T_f^{max}. Nucleation appeared to occur at random positions within the nanodroplets and without an induction period. The surface of the crystallized particle remains disordered, as previously reported in atomistic simulation studies of nanoscopic ice clusters.[31,34,41,65,66] We did not find evidence of preferential ice nucleation at the surface of the liquid

dx.doi.org/10.1021/ja210878c | J. Am. Chem. Soc. 2012, 134, 6650−6659

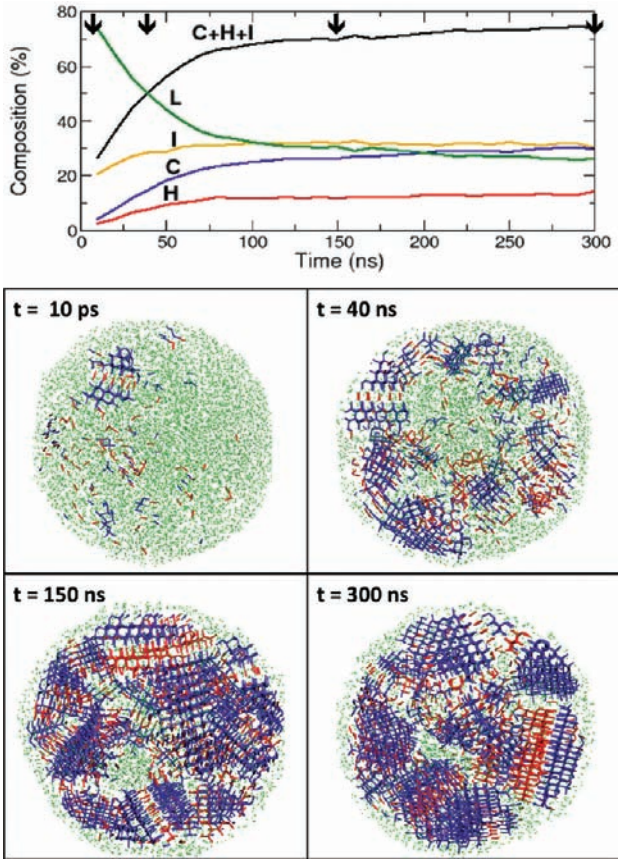

Figure 2. Freezing of a R = 4.7 nm water nanoparticle at T = 180 K. The upper panel shows the development of the percentage of cubic ice (blue), hexagonal ice (red), interfacial ice (orange), total ice (black), and liquid (green) over the 300 ns simulation. The arrows indicate the times for which the structures of the droplet are shown in the four lower panels. The cubic ice (blue lines), hexagonal ice (red lines), and liquid (green points) are shown; interfacial ice is hidden for clarity. It is apparent that at this temperature the crystallites are unable to consolidate to one large crystallite within 300 ns. The final ratio of cubic ice to hexagonal ice of this particular simulation is 2.2, which is also the average for this ensemble of 20 uncorrelated simulations of the R = 4.7 nm particles.

nanodroplets; larger sets of simulations (e.g., ∼100 per value of R) would be needed to determine the spatial distribution of critical nuclei in the nanoparticles. The freezing of water in the presence of a water−vapor interface has been investigated through atomistic simulations of slabs of water containing up to 600 molecules.[67] In that work, it was found that homogeneous freezing occurs at the subsurface, the layer of water just below the under-coordinated, disordered surface layer, but nucleation in the bulk of the slab was also observed. Another report, in which a model was fitted to experimental results of the freezing of micrometer-sized water droplets, indicated that surface nucleation becomes the dominant process for water droplets with R < 5 μm.[68] More recent studies, however, concluded that current experimental techniques cannot distinguish between surface and volume freezing in sub-micrometer aerosols[69] and micrometer-sized water droplets.[70]

The individual ice nuclei grow until they reach the boundary of neighboring crystallites, at which point they may consolidate into a larger crystallite or remain as several smaller crystallites separated by a thin layer of liquid. The ice crystallites in the nanoparticles consolidate as in bulk water, by direct attachment and rearrangement.[19] Direct attachment involves the consolidation of neighboring nuclei with already parallel stacking axes—the nuclei's planes of ice stacking are aligned such that the nuclei can merge without reorientation of the water molecules of any nucleus. Rearrangement, on the other hand, involves the reorientation of the stacking axis of one nucleus to match that of a neighboring nucleus in order to coalesce. Finally, nonconsolidation occurs when two nuclei have nonparallel stacking axes, are unable to rearrange, and grow independent crystallites separated by a thin layer of amorphous water. The latter scenario, with multiple crystallites of various sizes per nanoparticle, is the most common outcome of the isothermal crystallization at 180 K for the particles with R > 2 nm. Figure 3 displays randomly selected structures of crystallized clusters for all the sizes considered in this study.

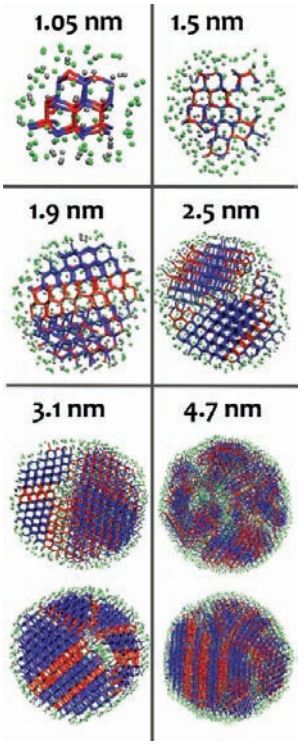

Figure 3. Structures of water nanoparticles crystallized at constant temperature. Randomly selected structures of water nanoparticles of different radii (indicated for each panel) crystallized under isothermal conditions at 150 K for R = 1.05 nm, 180 K for R = 1.5, 1.9, 2.5, 3.1, and 4.7 nm (the latter two are the upper figures of their panels), and 200 K for R = 3.1 and 4.7 nm (lower figures of their panels). The water molecules are colored according to whether they belong to the premelted liquid (green), interfacial ice (gray), cubic ice (blue), and hexagonal ice (red). The molecules with ordering of cubic and hexagonal ice are connected by sticks that represent hydrogen bonds. Crystallization from multiple nucleation sites in the largest nanoparticles at temperatures below T_f^{max} results in the formation of multiple ice crystallites separated by thin layers of liquid.

Crystallization of the water nanoparticles does not yield pure cubic ice, but rather a hybrid ice I with stacks of cubic and hexagonal ice layers. We note that the basal plane of hexagonal ice and the 111 plane of cubic ice are identical, allowing a seamless stacking of cubic and hexagonal layers. Previous simulations of bulk ice growth at 14 K supercooling indicate that these faults occur frequently.[71] The ratio of molecules with the local order of cubic ice with respect to those with local

dx.doi.org/10.1021/ja210878c | J. Am. Chem. Soc. 2012, 134, 6650−6659

order of hexagonal ice appears to be independent of droplet size and temperature, around 2.5 (Figure 4), and is comparable

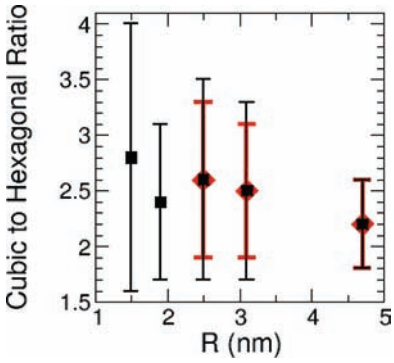

Figure 4. Ratio of cubic ice to hexagonal ice in the water nanoparticles. Ratios obtained from an ensemble of 20 isothermal simulations at 200 K (red diamonds) and 180 K (black squares) for each *R*-sized droplet. The ratio for R = 2.5 nm at 200 K was evaluated from 18 of 20 simulations, as the remaining two did not crystallize within 500 ns.

to the 2.3 cubic-to-hexagonal ratio for ice crystallized from bulk water at 180 K.[19] In none of the 160 simulations summarized in Figure 4 does hexagonal ice account for a greater percentage of a particle than cubic ice.

The hexagonal ice layers in the crystallites are largely growth and deformation faults occurring at random within the ice nanodroplets, as previously found for bulk and nanoconfined ice in experiments and simulations.[17,19,23,24,72] A growth fault is the incorporation of one hexagonal layer within a cubic ice sequence, and a deformation fault is the incorporation of two adjacent hexagonal layers within a cubic ice sequence. Less frequently, three or more consecutive hexagonal layers occurred within the droplets. We observed up to six adjacent hexagonal layers in a nanodroplet with R = 4.7 nm, and up to 15 consecutive cubic layers in another droplet of the same size. Growth and deformation stacking faults, as well as stacking of three adjacent hexagonal sequences, can be seen in the nanodroplets of Figures 2 and 3. The ratio of growth to deformation faults for the particles of this study is similar to the ratio for ice in nanopores, in which the number of growth faults significantly outnumber deformation faults:[24] analysis of the stacking faults at 200 K for $R \geq 2.5$ nm suggests the ratio may reach values greater than 7:1 in some droplets. The larger number of growth faults seems to be related to the formation of defects in the form of stacked water pentagons, recently reported in simulations of crystallization of bulk water,[51] at the boundaries of adjacent crystallites. Hexagonal ice growth faults then radiate from the edges of the pentagonal stacks (see, for example, the crystals in the R = 3.1 nm particles in Figure 3). A different type of defect consisting of coupled five- and eight-member rings was found to facilitate stacking faults in the growth of ice using a six-point model of water using a stationary temperature gradient.[73] We did not find the 5−8 defects in the nanoparticles. We note that a previous study of the formation of stacking faults in the growth of ice, also using simulations with the six-point water model, but without a temperature gradient, reported the same seamless stacking of hexagonal and cubic layers that we found for the nanoparticles and did not present 5−8 defects.[71] It is an open question whether the 5−8 defects of ref 73 are specific to certain growth conditions.

In the simulations discussed above the water nanoparticles were cooled at constant rate or evolved at constant temperature, conditions that could be achieved in experiments. Freezing of water nanoparticles in the atmosphere, however, could occur under conditions in which the particles are isolated. If ice were to grow at a rate much faster than the rate at which the heat of crystallization can be removed from a nanoparticle through collisions or evaporation, the crystallization would occur at constant energy, and the temperature would rise as ice forms. The upper panel of Figure 5 shows the evolution of the temperature of 4.7 nm radius nanoparticles that were equilibrated at temperatures ranging from 180 to 205 K and subsequently evolved at constant energy. The nanoparticles heated as a result of crystallization; evaporation was not

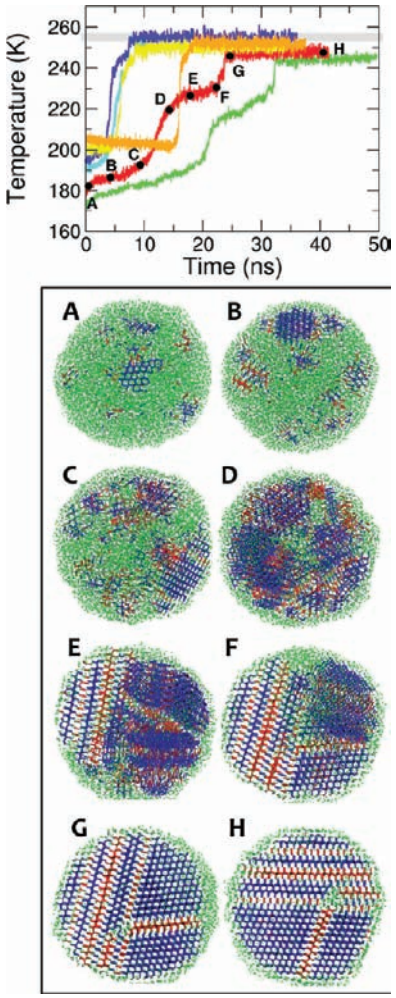

Figure 5. Isoenergetic crystallization of R = 4.7 nm nanoparticles. (Top) Temperature of nanoparticles evolved in microcanonical (*NVE*) simulations after being equilibrated for 0.1 ns at 170 (green), 180 (red), 190 (cyan), 195 (blue), 200 (yellow), and 205 K (orange). The crystallization heats up the particles, producing the melting of small ice crystallites and growth of the larger ones. The gray stripe indicates the melting temperature of the R = 4.7 nm particles. The crystallization is fastest at 195 K, consistent with the $T_f^{max} = 196 \pm 2$ K determined from the cooling simulations. (Bottom) Snapshots along the crystallization of the nanoparticle pre-equilibrated at 180 K at the times indicated by the letters in the upper panel. Molecules with the order of cubic (blue) and hexagonal (red) ice are connected by sticks representing the hydrogen bonds; liquid and interfacial ice are shown as green and gray balls, respectively.

dx.doi.org/10.1021/ja210878c | *J. Am. Chem. Soc.* 2012, 134, 6650−6659

observed. The final temperature of the nanoparticles depends on their energy but—consistent with the presence of ice—is always lower than or equal to the equilibrium melting temperature of the nanoparticles, which is independently determined in next section. The lower panel of Figure 5 shows the formation of ice in a particle pre-equilibrated at 180 K and evolved at constant energy. Same as in the isothermal crystallization at 180 K, independent crystallites grow from multiple nuclei. Different from the isothermal case, the growth leads to an increase in the temperature of the particle that favors the dissolution of the small crystallites and their recrystallization into larger ones. The process of reorganization and consolidation of crystallites inside the particle into a single crystal is the most pronounced as the temperature rises above 230 K. This process of Ostwald ripening within the nanoparticles is due to the strong dependence of the melting temperature of the crystallites with their size, which we address in next section.

3. Melting of the Crystallized Water Nanoparticles. We have shown that the structure of ice in the nanodroplets is neither pure cubic ice nor pure hexagonal ice but rather a hybrid ice I with stacks of each of the two polymorphs. We now investigate whether the ratio of cubic to hexagonal ice within a droplet affects its melting temperature, whether the ice in the particles transforms into pure hexagonal ice before melting, and what is the dependence of the equilibrium melting temperature with the particle radius. The melting temperature of each of the crystallized nanodroplets was determined by heating the nanoparticle at a constant rate of 1 K ns^{-1}, as shown in Figure 6. Different from the freezing process, the melting of the nanoparticles occurs at the liquid–ice equilibrium temperature, without superheating, due to the existence of a premelted liquid layer in the crystallized nanoparticles.

We find a significant depression of the melting temperatures with decreasing radii of the particles (Table 1). The melting temperatures $T_m(R)$ are very well represented, see Figure 1, by the Gibbs–Thomson equation,[62,63] $T_m(R) = T_m^{bulk} - K_{GT}/(R - d)$, where $T_m^{bulk} = 274$ K is the bulk melting temperature for the mW model,[42,74] $d = 0.26 \pm 0.05$ nm is the thickness of the premelted layer, and $K_{GT} = 82 \pm 5$ K·nm is the Gibbs–Thomson constant. The width of the premelted layer predicted from the melting temperatures is about one water diameter, consistent with the amount of liquid covering the ice observed in the structure of the crystallized nanoparticles. The theoretical expression of the Gibbs–Thomson constant for melting is $K_{GT} = \alpha T_m^{bulk} \gamma_{sl} V_s / \Delta H_m$, where $\alpha = 3$ for spherical particles and 2 for cylinders, ΔH_m is the molar enthalpy of melting of ice, γ_{sl} is the liquid–ice surface tension, and V_s is the molar volume of ice.[62] K_{GT} predicted from the experimental bulk properties of water and using $\alpha = 3$ is 78.6 K·nm, indistinguishable from the 82 ± 5 K·nm determined from the $T_m(R)$ in the simulations. Similarly, the K_{GT} determined from melting of ice in cylindrical nanopores with the mW model is 54 K·nm,[24,75] in excellent agreement with the 52 K·nm determined from experiments[76] and the 52 K·nm predicted by the expression above with $\alpha = 2$. We find that K_{GT} and d obtained by fitting the Gibbs–Thomson equation to the T_m obtained in the mW simulations perfectly reproduce (within the 3 K error bars) the depression in the melting point, $\Delta T_m = T_m(R) - T_m^{bulk}$, determined for purely hexagonal ice clusters with $N = 768$, 2592, 6144, and 9600 molecules in simulations with the TIP4P[77] water model.[41] This is remarkable because the melting point of the TIP4P model is 230 K and its enthalpy of melting ΔH_m is 73% of the experimental value,[78] while for mW water $T_m = 274$ K and ΔH_m is 87% of the experimental value. At odds with the assumptions used in the derivation of the Gibbs–Thomson equation, we find that the enthalpy of melting is not constant with particle size. The enthalpy of melting of the $R = 1.05$ nm droplets is about 1 kJ mol^{-1} (about 2 kJ mol^{-1} if only the ice is considered in the normalization), significantly lower than the 5.3 kJ mol^{-1} measured for bulk mW water at 274 K.[42] The small ΔH_m measured for the smallest droplets is consistent with the low value of the excess enthalpy of amorphous water over ice at 170 K, which is about 2.2 kJ mol^{-1} for mW water[45] and 1.5 kJ mol^{-1} in experiments.[79] These results suggest that the robust values of K_{GT} among models and their agreement with the predictions using experimental data for bulk water could

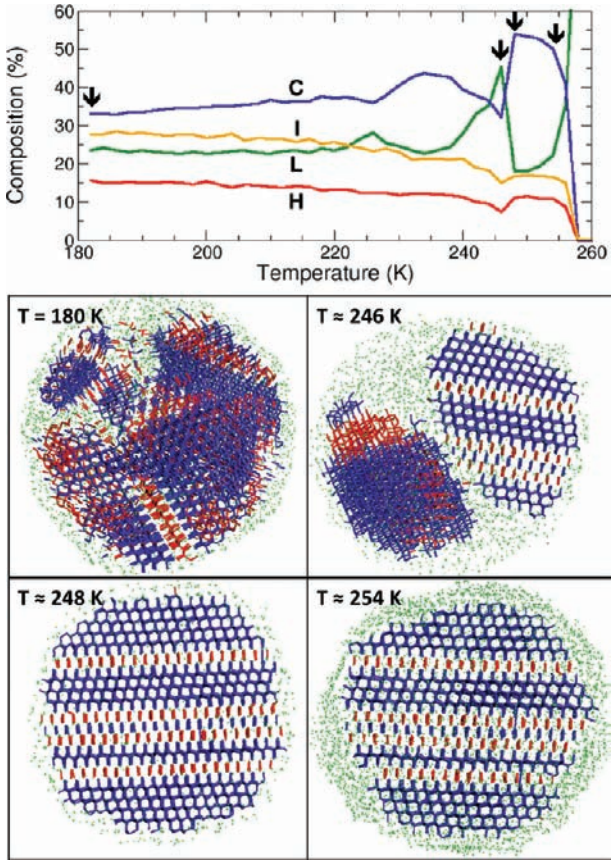

Figure 6. Ostwald ripening and melting of ice in $R = 4.7$ nm particle upon heating at a rate of 1 K ns^{-1}. The uppermost figure shows the evolution of cubic ice (blue line), hexagonal ice (red line), interfacial ice (orange line), and liquid (green line) as a function of temperature. The arrows signal the temperatures for which the structures are shown in the lower panel. The crystallized droplet obtained by cooling the water cluster at 1 K ns^{-1} had multiple crystallites, as seen in the structure at $T = 180$ K. Hydrogen bonds between water molecules characterized as cubic ice are shown by blue lines, red lines show hydrogen bonds between waters with the order of hexagonal ice, and liquid water is represented by green points. For clarity, interfacial ice is not shown. The melting of the smallest crystallites produces an increase in the fraction of liquid, which reaches a local maximum at 246 K, followed by growth of the largest crystallites within the droplet, producing a single crystallite before melting. At 248 K (lower left panel) the fraction of liquid is at minimum, and a single droplet with stacking faults but no other defects is formed, before the droplet finally melts. By $T \approx 254$ K (lower right panel) melting has begun, with ice melting first at or near the surface and advancing toward the core of the water particle.

dx.doi.org/10.1021/ja210878c | J. Am. Chem. Soc. 2012, 134, 6650–6659

originate in a proportionality in the enthalpy of melting and liquid−ice surface tension. Using Turnbull's heuristic relation between the heat of melting and the surface tension,[80] $\gamma_{sl} = \Delta H_m V_m^{-2/3}$ (where $\lambda = 0.32$ for water), Jähnert et al. showed that the Gibbs−Thomson constant can be simplified to an expression that depends only on the bulk melting temperature and the molecular volume, $K_{GT} = \alpha\lambda T_m^{bulk} v^{1/3}$.[80] This simplified equation suggests that the agreement in the predicted $\Delta T_m = T_m(R) - T_m^{bulk}$ across models may be rooted in the relative insensitivity of the volume of water to temperature.[61]

Table 1 shows that the dispersion in the melting temperatures of the 20 droplets for each R is just 1%, although the crystals from which they melt have a wide distribution of ratio of cubic to hexagonal layers. The only exceptions are the R = 1.05 nm particles, for which the dispersion is about 5% and stacks are not well developed. We conclude that the stacking patterns of ice have little effect on the melting temperature of the water particles. To further evaluate whether the hybrid ice I forms because it is more stable than hexagonal ice, we determined the melting temperature of pure hexagonal ice crystallites of the same radii as the nanoparticles of this study. We found that the droplets of pure hexagonal ice have a melting temperature indistinguishable, within the 1% uncertainty, from that of the ice droplets with cubic and hexagonal stacking (Table 1). We also determined the melting temperature for a purely cubic crystallite with R = 4.7 nm and found it to be 256 ± 2 K, indistinguishable from the pure Ih (257 ± 2 K) and hybrid crystallites (255 ± 2 K). These results indicate that the stacking ratio of cubic ice to hexagonal ice has little effect on the free energy of the ice.[19,24,71]

Heating of the multicrystalline ice particles at a constant rate produces the dissolution of the smaller (less stable) ice crystallites to grow the larger crystallites. This process of Ostwald ripening is most pronounced at temperatures about 30 K to 3 K below the melting point of the nanoparticle and is illustrated in Figures 5 and 6 for isoenergetic and constant heating rate simulations, respectively. Figure 6 shows that the fraction of liquid within a multicrystalline nanoparticle heated at a constant rate increases until T as near as 3 K below the melting point, at which point there is an *increase in the amount of ice on heating* as the small crystallites dissolve on reaching their corresponding melting temperature, leading to a growth of the larger crystallites, which are still at a temperature below their melting points. This results in the formation of a single large ice crystallite, which finally melts on further heating. The melting of the water nanoparticles proceeds from the surface toward the interior, in contrast to the freezing process, which occurs through all the volume of the droplet. Ostwald ripening within the droplets was observed for all heating simulations of droplets that contain multiple crystallites (those with R > 1.9 nm). For the 1.9 nm droplets, 18 of 20 initial ice structures already contained only one crystallite, not allowing for crystallite reorganization and annealing. The fact that just below the melting temperature all droplets have annealed to single crystals (albeit with plenty of stacking faults) explains the very low dispersion in the values of T_m observed for the sets of 20 independent simulations for each R: it is the size of the crystallites, and not their stacking faults what impacts their equilibrium melting temperature.

It is important to note that the reorganization of the ice structure on approaching the melting temperature of the nanoparticle does not involve the loss of the cubic ice layers. The ratio of molecules with the order of cubic ice (C) to molecules with the order of hexagonal ice (H) changes, usually increases, during the ripening process. For instance, for the R = 4.7 nm droplets, the ratio C/H = 2.1 ± 0.4 at 180 K after cooling, but C/H = 3.2 ± 1.4 for the structures with the largest fractions of ice along the heating trajectory. Direct melting from hybrid ice with stacks of cubic and hexagonal ice layers to the liquid, without a prior transformation to hexagonal ice, has been previously reported in experiments and simulations of water in nanopores.[22−24,81,82] The results of the present study indicate that, likewise, melting of the ice nanoparticles does not involve an intermediate step of transformation to pure hexagonal ice. The absence of spectroscopic evidence of hexagonal ice in nanodroplets supports the scenario predicted by the simulations of this study.

CONCLUSIONS

We investigated the freezing, melting, and structure of ice formed by water nanoparticles with radii ranging from about 1 to 5 nm using molecular dynamics simulations. Through analysis of several hundred independent simulations of freezing and melting, we investigated the microscopic process of nucleation and growth of the crystallites and their Ostwald ripening, characterized the structure of the ice and the width of the premelted layer, computed equilibrium melting temperatures and nonequilibrium freezing temperatures, and estimated the crystallization rates of the nanoparticles. To the best of our knowledge, this is the first molecular simulation study that reports the crystallization and structure of ice in nanoparticles with more than 20 molecules.

Our results suggest that atmospheric ice nanoparticles do not have the structure of Ih or Ic, but rather a hybrid ice I containing short stacks of cubic and hexagonal ice layers in a ratio of about 2:1. This ratio seems to be quite insensitive to the size of the droplet and similar to the ratio observed for the crystallization of water in bulk and in nanopores in the same temperature range.[19,24] The equilibrium melting temperatures of the ice nanoparticles with hybrid or hexagonal ice structure are indistinguishable within the 1% error bar of the simulations, suggesting that the stacking has little effect on the free energy of the confined ice. It has been shown elsewhere that the diffraction patterns of these hybrid ice crystals are very similar to the diffraction pattern expected for cubic ice.[17−21] The broadening of the diffraction peaks that results from the small size of the crystals poses an additional challenge for the distinction of hybrid ice I from true ice Ic nanoparticles in experiments.

The simulations indicate that melting of the nanodroplets involves a transition from hybrid ice I to liquid, without the formation of an intermediate hexagonal ice phase. Our results are consistent with the absence of spectroscopic evidence for hexagonal ice nanoparticles in experiments, and are similar to what was previously reported for melting of ice in nanopores.[22−24,81,82] These results pose the question of whether the hybrid ice I structure could be the stable phase of nanoconfined ice. Johari has predicted that water particles with R > 15 nm would favor hexagonal ice, and smaller ones would be cubic.[83] Transformation hybrid ice I to ice Ih before melting has been reported for bulk[17] and micrometer-sized ice droplets.[6,16] Free energy calculations and accurate experimental determinations of the structure of ice in water nanoparticles as a function of size and temperature would be invaluable for establishing the conditions for which hexagonal ice becomes the stable crystal of confined water.

The melting temperatures sharply decrease with the radius of the water crystals in a manner well represented by the Gibbs−Thomson equation. The strong variation of the melting temperature with radius is responsible for the Ostwald ripening observed for the crystallites within each nanoparticle as the temperature approaches the particle's melting point. The width of the premelted layer deduced from the Gibbs−Thomson relation is $d = 0.26 \pm 0.05$ nm, about a monolayer, in agreement with the amount and location of liquid observed from direct examination of the structure of the crystallized nanoparticles. Disordered water at the surface of the particles was found down to the lowest temperatures of this study, consistent with previous reports on premelting of ice in bulk, in nanoparticles, and confined in nanopores.[24,25,41,61,66,84−90] The disordered layer of water entirely covers the surface of the ice nanoparticles, therefore it is of particular relevance for chemical reactions on atmospheric water particles.[4]

The steepness of the decrease of the melting temperature with radius is given by the value of the Gibbs−Thomson constant K_{GT}. The value obtained from the simulations, $K_{GT} = 82 \pm 5$ K·nm, is in excellent agreement with the value predicted from experimental thermodynamic data for bulk water at the melting point, 78.6 K·nm. However, at odds with the assumptions made in the derivation of the Gibbs−Thomson equation, we find that the enthalpy of melting decreases with the size of the particle. The enthalpy of melting for the $R = 1.05$ nm nanoparticles is about a quarter of the bulk value of ΔH_m at T_m^{bulk}. This suggests that the liquid−ice surface tension also decreases for small cluster radii. The diminished apparent value of ΔH_m for the smaller nanoparticles results both from the significant fraction of premelted liquid in the particles and the decrease in the excess enthalpy of liquid water with respect to ice at low temperatures. We find that water clusters as small as 137 molecules, $R = 1.0$ nm, can still produce a tiny crystallite at 150 K, which dissolves and re-forms during simulations spanning several hundreds of nanoseconds. The extrapolated melting line $T_m(R)$ would cross the bulk glass transition temperature $T_g = 136$ K for clusters with $N \approx 100$ molecules, a size that also corresponds to the critical nucleus of bulk water close to the temperature of homogeneous nucleation.[45] That extrapolation and the small fraction of cubic and hexagonal ice in the crystallized $R = 1.0$ and 1.05 nm nanoparticles suggests that clusters with about 100 water molecules or less would be amorphous, in agreement with previous predictions in the literature.[10,31,50,65]

The temperature of maximum crystallization rate T_f^{max} of the water nanoparticles decreases with decreasing radii, but their dependence with droplet size is less pronounced than for the equilibrium melting transition. We find that the freezing temperatures are also well described by a modified Gibbs−Thomson equation, although that relation is derived from equilibrium thermodynamics and freezing is a nonequilibrium process. The existence of an underlying structural (thermodynamic) transformation in the liquid that controls the rate of ice crystallization[45] may explain the ability of an equation derived from phase equilibrium for predicting the nonequilibrium freezing temperatures of water.

The liquid−ice phase diagram derived in this work provides a framework to interpret the structure and phase transformation of water nanoparticles in the atmosphere. Determination of the glass transition temperatures as a function of droplet size would be important to predict the state—vitreous or crystalline—of water nanoparticles at the cold temperatures prevalent in the polar mesosphere. Atmospheric particles and aerosols are also known to contain ions, in the form of nitric acid, sulfuric acid, and various salts and organic compounds.[1,2,4] Experimental studies indicate that a high concentration of acids inhibits or slows down the crystallization of ice in micrometer-sized droplets.[5] The interplay of kinetic and thermodynamic factors in the crystallization of ice in aqueous nanodroplets containing solutes is an open question that deserves further study.

AUTHOR INFORMATION

Corresponding Author

Valeria.Molinero@utah.edu

Notes

The authors declare no competing financial interest.

ACKNOWLEDGMENTS

This work was supported by the Arnold and Mabel Beckman Foundation through a Young Investigator Award to V.M. We thank the Center of High Performance Computing of the University of Utah for allocation of computing time.

REFERENCES

(1) Klemperer, W.; Vaida, V. *Proc. Natl. Acad. Sci. U.S.A.* **2006**, *103*, 10584−10588.
(2) Kulmala, M. *Science* **2003**, *302*, 1000−1001.
(3) Hock, C.; Schmidt, M.; Kuhnen, R.; Bartels, C.; Ma, L.; Haberland, H.; v. Issendorff, B. *Phys. Rev. Lett.* **2009**, *103*, 73401.
(4) Vaida, V. *J. Chem. Phys.* **2011**, *135*, 020901.
(5) Murray, B. J. *Atmos. Chem. Phys. Discuss.* **2008**, *8*, 8743−8771.
(6) Murray, B. J.; Knopf, D. A.; Bertram, A. K. *Nature* **2005**, *434*, 202−205.
(7) Lübken, F.-J.; Lautenbach, J.; Höffner, J.; Rapp, M.; Zecha, M. *J. Atmos. Solar-Terrestrial Phys.* **2009**, *71*, 453−463.
(8) Murphy, D. M. *Geophys. Res. Lett.* **2003**, *30*, 17.
(9) Ostwald, W. *Z. Phys. Chem.* **1897**, *22*, 289−302.
(10) Zasetsky, A. Y.; Petelina, S. V.; Svishchev, I. M. *Atmos. Chem. Phys* **2009**, *9*, 965−971.
(11) Murray, B. J.; Jensen, E. J. *J. Atmos. Solar-Terrestrial Phys.* **2010**, *72*, 51−61.
(12) Konig, H. *Z. Kristallogr.* **1943**, *105*, 279−286.
(13) Whalley, E. *Science* **1981**, *211*, 389−390.
(14) Goodman, J.; Toon, O. B.; Pueschel, R. F.; Snetsinger, K. G.; Verma, S. *J. Geophys. Res.* **1989**, *94*, 16449−16457.
(15) Riikonen, M.; Sillanpää, M.; Virta, L.; Sullivan, D.; Moilanen, J.; Luukkonen, I. *Appl. Opt.* **2000**, *39*, 6080−6085.
(16) Murray, B. J.; Bertram, A. K. *Phys. Chem. Chem. Phys.* **2006**, *8*, 186−192.
(17) Hansen, T. C.; Koza, M. M.; Kuhs, W. F. *J. Phys.: Condens. Matter* **2008**, *20*, 285104.
(18) Hansen, T. C.; Falenty, A.; Kuhs, W. F. In *Physics and Chemistry of Ice*; Kuhs, W. F., Ed.; RSC Publishing, Royal Society of Chemistry: Cambridge, UK, 2006; pp p 201−208.
(19) Moore, E. B.; Molinero, V. *Phys. Chem. Chem. Phys.* **2011**, *13*, 20008−20016.
(20) Kuhs, W. F.; Bliss, D. V.; Finney, J. L. *J. Phys. Colloques* **1987**, *48*, 631−636.
(21) Malkin, T. L.; Murray, B. J.; Brukhno, A. V.; Anwar, J.; Salzmann, C. G. *Proc. Natl. Acad. Sci. U.S.A.* **2012**, *109*, 1041−1045.
(22) Morishige, K.; Yasunaga, H.; Uematsu, H. *J. Phys. Chem. C* **2009**, *113*, 3056−3061.
(23) Morishige, K.; Uematsu, H. *J. Chem. Phys.* **2005**, *122*, 044711.
(24) Moore, E. B.; de la Llave, E.; Welke, K.; Scherlis, D. A.; Molinero, V. *Phys. Chem. Chem. Phys.* **2010**, *12*, 4124−4134.
(25) González Solveyra, E.; De La Llave, E.; Scherlis, D. A.; Molinero, V. *J. Phys. Chem. B* **2011**, *115*, 14196−14204.

(26) Sippel, C.; Hansen, T. C.; Koza, M. M.; Kuhs, W. F. *Geophysical Research Abstracts*, 13th EGU General Assembly, 2011.
(27) Huang, J.; Bartell, L. S. *J. Phys. Chem.* **1995**, *99*, 3924−3931.
(28) Bartell, L. S.; Huang, J. *J. Phys. Chem.* **1994**, *98*, 7455−7457.
(29) Torchet, G.; Schwartz, P.; Farges, J.; de Feraudy, M. F.; Raoult, B. *J. Chem. Phys.* **1983**, *79*, 6196.
(30) Stein, G. D.; Armstrong, J. A. *J. Chem. Phys.* **1973**, *58*, 1999−2003.
(31) Devlin, J. P.; Joyce, C.; Buch, V. *J. Phys. Chem. A* **2000**, *104*, 1974−1977.
(32) Wyslouzil, B. E.; Wilemski, G.; Strey, R.; Seifert, S.; Winans, R. E. *Phys. Chem. Chem. Phys.* **2007**, *9*, 5353−8.
(33) Kim, Y.; Wyslouzil, B.; Wilemski, G.; Wolk, J.; Strey, R. *J. Phys. Chem. A* **2004**, *108*, 4365−4377.
(34) Bartell, L. S.; Chushak, Y. G. In *Water in Confining Geometries*; Buch, V., Devlin, J. P., Eds.; Springer-Verlag: Berlin/Heidelberg, 2003.
(35) Manka, A.; Pathak, H.; Tanimura, S.; Wölk, J.; Strey, R.; Wyslouzil, B. E. *Phys. Chem. Chem. Phys.* **2012**, *14*, 4505−4516.
(36) Tsai, C. J.; Jordan, K. D. *J. Chem. Phys.* **1991**, *95*, 3850−3853.
(37) Kaneko, T.; Akimoto, T.; Yasuoka, K.; Mitsutake, A.; Zeng, X. C. *J. Chem. Theory Comput.* **2011**, *7*, 3083−3087.
(38) Laria, D.; Rodriguez, J.; Dellago, C.; Chandler, D. *J. Phys. Chem. A* **2001**, *105*, 2646−2651.
(39) Egorov, A. V.; Brodskaya, E. N.; Laaksonen, A. *Mol. Phys.* **2001**, *100*, 941−951.
(40) Egorov, A. V.; Brodskaya, E. N.; Laaksonen, A. *J. Comput. Theor. Nanosci.* **2008**, *5*, 1914−1922.
(41) Pan, D.; Liu, L. M.; Slater, B.; Michaelides, A.; Wang, E. *ACS Nano* **2011**, *5*, 4562−4569.
(42) Molinero, V.; Moore, E. B. *J. Phys. Chem. B* **2009**, *113*, 4008−4016.
(43) Moore, E. B.; Molinero, V. *J. Chem. Phys.* **2009**, *130*, 244505.
(44) Moore, E. B.; Molinero, V. *J. Chem. Phys.* **2010**, *132*, 244504.
(45) Moore, E. B.; Molinero, V. *Nature* **2011**, *479*, 506−508.
(46) Kastelowitz, N.; Johnston, J. C.; Molinero, V. *J. Chem. Phys.* **2010**, *132*, 124511.
(47) Johnston, J. C.; Kastelowitz, N.; Molinero, V. *J. Chem. Phys.* **2010**, *133*, 154516.
(48) Plimpton, S. J. *J. Comput. Phys.* **1995**, *117*, 1.
(49) Tanaka, H. *Phys. Rev. E* **2003**, *68*, 115051−115058.
(50) Buch, V.; Sigurd, B.; Devlin, J. P.; Buck, U.; Kazimirski, J. K. *Int. Rev. Phys. Chem.* **2004**, *23*, 375−433.
(51) Li, T.; Donadio, D.; Russo, G.; Galli, G. *Phys. Chem. Chem. Phys.* **2011**, 13.
(52) Reinhardt, A.; Doye, J. P. K *J. Chem. Phys.* **2012**, *136*, 054501.
(53) Cooper, S.; Nicholson, C.; Liu, J. *J. Chem. Phys.* **2008**, *129*, 124715.
(54) Liu, J.; Nicholson, C. E.; Cooper, S. J. *Langmuir* **2007**, *23*, 7286−7292.
(55) Li, Z. H.; Truhlar, D. G. *J. Am. Chem. Soc.* **2008**, *130*, 12698−12711.
(56) Kunz, R.; Berry, R. *Phys. Rev. E* **1994**, *49*, 1895−1908.
(57) Wales, D.; Berry, R. *Phys. Rev. Lett.* **1994**, *73*, 2875−2878.
(58) Berry, R. S.; Smirnov, B. A. *Int. J. Mass Spectrom.* **2009**, *280*, 204−208.
(59) Berry, R.; Smirnov, B. *Entropy* **2010**, *12*, 1303−1324.
(60) Findenegg, G.; Jähnert, S.; Akcakayiran, D.; Schreiber, A. *ChemPhysChem* **2008**, *9*, 2651−2659.
(61) Jahnert, S.; Chavez, F. V.; Schaumann, G. E.; Schreiber, A.; Schonhoff, M.; Findenegg, G. H. *Phys. Chem. Chem. Phys.* **2008**, *10*, 6039−6051.
(62) Christenson, H. K. *J. Phys.: Condens. Matter* **2001**, *13*, R95−R133.
(63) Petrov, O. V.; Furó, I. *Prog. Nucl. Magn. Reson. Spectrosc.* **2009**, *54*, 97−122.
(64) Koop, T.; Luo, B. P.; Tsias, A.; Peter, T. *Nature* **2000**, *406*, 611−614.
(65) Devlin, J. P.; Buch, V. *J. Phys. Chem. B* **1997**, *101*, 6095−6098.
(66) Pereyra, R. G.; Carignano, M. A. *J. Phys. Chem. C* **2009**, *113*, 12699−12705.
(67) Vrbka, L.; Jungwirth, P. *J. Phys. Chem. B* **2006**, *110*, 18126−18129.
(68) Kuhn, T.; Earle, M. E.; Khalizov, A.; Sloan, J. J. *Atmos. Chem. Phys.* **2011**, *11*, 2853−2861.
(69) Sigurbjörnsson, Ó. F.; Signorell, R. *Phys. Rev. E* **2008**, *77*, 05601.
(70) Stan, C. A.; Schneider, G. F.; Shevkoplyas, S. S.; Hashimoto, M.; Ibanescu, M.; Wiley, B. J.; Whitesides, G. M. *Lab Chip* **2009**, *9*, 2293−2305.
(71) Carignano, M. A. *J. Phys. Chem. C* **2007**, *111*, 501−504.
(72) Brukhno, A. V.; Anwar, J.; Davidchack, R.; Handel, R. *J. Phys.: Condensed Matter* **2008**, *20*, 494243.
(73) Pirzadeh, P.; Kusalik, P. *J. Am. Chem. Soc.* **2011**, *133*, 704−707.
(74) Jacobson, L. C.; Hujo, W.; Molinero, V. *J. Phys. Chem. B* **2009**, *113*, 10298−10307.
(75) De La Llave, E.; Gonzalez-Solveyra, E.; Scherlis, D. A.; Molinero, V. Manuscript in preparation.
(76) Schreiber, A.; Ketelsen, I.; Findenegg, G. H. *Phys. Chem. Chem. Phys.* **2001**, *3*, 1185−1195.
(77) Jorgensen, W. L.; Chandrasekhar, J.; Madura, J. D.; Impey, R. W.; Klein, M. L. *J. Chem. Phys.* **1983**, *79*, 926−935.
(78) Abascal, J. L. F.; Sanz, E.; Fernandez, R. G.; Vega, C. *J. Chem. Phys.* **2005**, *122*, 234511.
(79) Johari, G. P.; Fleissner, G.; Hallburcker, A.; Mayer, E. *J. Phys. Chem.* **1994**, *98*, 4719−4725.
(80) Turnbull, D. *J. Appl. Phys.* **1950**, *21*, 1022−1028.
(81) Webber, J.; Dore, J.; Strange, J.; Anderson, R.; Tohidi, B. *J. Phys.: Condensed Matter* **2007**, *19*, 415117.
(82) Jelassi, J.; Castricum, H. L.; Bellissent-Funel, M.-C.; Dore, J.; Webber, J. B. W.; Sridi-Dorbez, R. *Phys. Chem. Chem. Phys.* **2010**, *12*, 2838.
(83) Johari, G. P. *J. Chem. Phys.* **2005**, *122*, 194504.
(84) Dash, J. G.; Rempel, A. W.; Wettlaufer, J. S. *Rev. Mod. Phys.* **2006**, *78*, 695−741.
(85) Li, Y.; Somorjai, G. A. *J. Phys. Chem. C* **2007**, *111*, 9631−9637.
(86) Liu, E.; Dore, J. C.; Webber, J. B. W.; Khushalani, D.; Jähnert, S.; Findenegg, G. H.; Hansen, T. *J. Phys.: Condens. Matter* **2006**, *18*, 10009−10028.
(87) Conde, M. M.; Vega, C.; Patrykiejew, A. *J. Chem. Phys.* **2008**, *129*, 014702.
(88) Paesani, F.; Voth, G. *J. Phys. Chem. C* **2008**, *112*, 324−327.
(89) Neshyba, S.; Nugent, E.; Roeselová, M.; Jungwirth, P. *J. Phys. Chem. C* **2009**, *113*, 4597−4604.
(90) Moore, E. B.; Allen, J. T.; Molinero, V. *J. Phys. Chem. C* **2012**, *116*, 7507−7514.